Vortex lattices in strongly confined quantum droplets

T. A. Yoğurt [1,*] U. Tanyeri [1] A. Keleş [1] and M. Ö. Oktel [2]
[1]*Department of Physics, Middle East Technical University, Ankara 06800, Turkey*
[2]*Department of Physics, Bilkent University, Ankara 06800, Turkey*

(Received 4 August 2023; accepted 8 September 2023; published 25 September 2023)

Bose mixture quantum droplets display a fascinating stability that relies on quantum fluctuations to prevent collapse driven by mean-field effects. Most droplet research focuses on untrapped or weakly trapped scenarios, where the droplets exhibit a liquidlike flat density profile. When weakly trapped droplets rotate, they usually respond through center-of-mass motion or splitting instability. Here, we study rapidly rotating droplets in the strong external confinement limit where the external potential prevents splitting and the center-of-mass excitation. We find that quantum droplets form a triangular vortex lattice as in single-component repulsive Bose-Einstein condensates (BECs), but the overall density follows the analytical Thomas-Fermi profile obtained from a cubic equation. We observe three significant differences between rapidly rotating droplets and repulsive BECs. First, the vortex core size changes markedly at finite density, visible in numerically obtained density profiles. We analytically estimate the vortex core sizes from the droplets' coherence length and find good agreement with the numerical results. Second, the change in the density profile gives a slight but observable distortion to the lattice, which agrees with the distortion expected due to nonuniform superfluid density. Lastly, unlike a repulsive BEC, which expands substantially as the rotation frequency approaches the trapping frequency, rapidly rotating droplets show only a fractional change in their size. We argue that this last point can be used to create clouds with lower filling factors, which may facilitate reaching the elusive strongly correlated regime.

DOI: 10.1103/PhysRevA.108.033315

I. INTRODUCTION

Rotating a Bose-Einstein condensate (BEC) results in nonclassical phenomena due to the irrotational nature of superfluid flow in the absence of density singularities [1,2]. A phase-coherent BEC carries angular momentum through quantized vortices, forming a regular vortex lattice to mimic solid body rotation. Single-component BECs with repulsive interactions were experimentally observed to create a triangular lattice of singly quantized vortices when rotated in an isotropic harmonic trap [3–5]. The rotation frequency and superfluid density dependence of the vortex core size, vortex density, and condensate radius of the rotating repulsive BECs are theoretically studied for both the Thomas-Fermi (TF) and the lowest Landau-level (LLL) regimes [6]. On the other hand, BECs of attractively interacting atoms are only metastable under harmonic confinement, and they carry angular momentum via center-of-mass (COM) rotation rather than vortices [7].

Vortex lattices of two-component BEC mixtures were investigated for various intracomponent g_{11} and g_{22} and intercomponent g_{12} interactions [6,8–11]. Depending on the strength of the repulsive $g_{12} > 0$, the mixture can exhibit coincident or displaced lattices with triangular, square, or rectangular symmetries. For the attractive intercomponent $g_{12} < 0$ and mechanically stable $|g_{12}| < \sqrt{g_{11}g_{22}}$ Bose mixtures, both components coincide and form a triangular lattice [8]. However, the mean-field (MF) treatment of the Bose mixture problem predicts that the condensate is unstable towards collapse for $g_{12} < 0$ and $|g_{12}| < \sqrt{g_{11}g_{22}}$ [1]. The mixture can be metastable for a small number of particles if it is confined by a harmonic trap.

Quantum fluctuations can drastically modify the mean-field prediction toward collapse. Bose mixture quantum droplets are mechanically stable self-trapped phases without any external confinement, where attractive MF interaction $\propto -\delta g n^2$ is countered by the effectively repulsive beyond mean-field (BMF) fluctuations $\propto g_{\mathrm{BMF}} n^{5/2}$ [12]. Here, $\delta g = |g_{12}| - \sqrt{g_{11}g_{22}}$ and n is the condensate density. For large particle numbers N, the interaction energy dominates the ground state, and the equilibrium density profile is almost like an incompressible liquid with a constant density [12]. For smaller N, the droplet can still stabilize itself, but the ground state exhibits a smoothly decaying density profile. There is a critical particle number below which the kinetic-energy cost is too large and the droplet cannot sustain itself against expansion if it is not trapped.

The quantum droplet has features of both the attractively interacting BEC due to mean-field energy and the repulsively interacting BEC due to quantum fluctuation. The response of a quantum droplet to rotation is not straightforward. Specifically, the competition between the mean-field interaction and the quantum fluctuations gives rise to a new length scale, which is determined by the droplet's equilibrium density. Recent investigations of the problem mainly concentrated on the unconfined or weakly trapped droplet. Angular momentum is primarily carried by the COM rotation for the liquidlike flat-density droplets in free space or weak external confinement

*ayogurt@metu.edu.tr

[13–15]. This way, the droplet conserves the ground-state interaction energy by preserving the flat-top density profile. By the same physical reasoning, the droplets experience splitting instability under a density perturbation, i.e., the droplet tends to break into smaller fragments [16–19]. However, vortices can be locally stable within the unconfined flat-top droplets if phase imprinted [16,17] or the external confinement is adiabatically removed [18]. Even weak confinement can help avoid splitting instability and make vortex states stable. A rotating droplet under harmonic confinement is recently predicted to show a combination of COM rotation and vortex states [13,14].

The literature on quantum droplets mostly focuses on their self-trapping property, making the confinement potential mostly irrelevant. Here, we classify the physical regimes for a trapped droplet by investigating the energy scales in the problem. Relative strengths of the potential and interaction energies and the interplay between the free equilibrium density and particle number decide the significance of the confining potential for the rotating problem. We argue that a strongly confined droplet can be driven into the rapidly rotating regime, forming a large vortex lattice.

We study such rapidly rotating droplets in the strongly confined TF regime by numerical and approximate analytical methods. We numerically find that the confined droplet exhibits a triangular vortex lattice under rapid rotation. Strong confinement ensures that the splitting instability is avoided even when the rotation frequency is close to the trap frequency. The density profile of the vortex lattice closely follows the TF profile, with a convex peak at the center and a rapid fall at the TF radius. As the rotation frequency approaches trapping frequency $\tilde{\Omega} \to 1$, the effective confinement $\propto (1-\tilde{\Omega}^2)$ weakens, and the density profile of the vortex lattice converges to flat-top droplet density. Contrary to the diverging size of rapidly rotating repulsive BECs [20,21], the strongly confined TF droplet converges to a finite radius at the limit $\tilde{\Omega} \to 1$. Thus, the physics of self-trapping plays an important role in the rapid rotation limit.

Our numerical simulations show that the vortex core sizes near the center and the edge of the droplet are noticeably different. We develop an approximate analytical formula for the density dependence of the core size. The vortex cores in the repulsive BECs scale as $\zeta \propto 1/\sqrt{n_0}$, where n_0 is the condensate density. For the strongly confined TF droplet, however, we find the core size $\zeta \propto \frac{1}{\sqrt{n_0}\sqrt{n_0^{1/2}-n_c^{1/2}}}$, where the pole in the denominator n_c is approximately equal to the equilibrium density of the unconfined droplet. The divergence at a finite density creates an observable difference in the core size in different regions of the vortex lattice. We also calculate the deviation of the vortex lattice from a perfect triangular lattice. While this deviation remains small, it is observable and agrees with numerical results. Finally, we argue that the rapidly rotating droplets present an opportunity to realize BECs where the number of particles is within an order of magnitude of the number of vortices in the condensate. While the Gross-Pitaevskii (GP) equation and our assumptions about local energy of fluctuations are expected to break down in this limit, we argue that rapidly rotating droplets may facilitate reaching the strongly correlated regime.

This paper is organized as follows. In Sec. II, we introduce the effective GP equation of mixture droplets and tabulate different parameter regimes of the problem. In Sec. III, we discuss the TF solution for the strongly confined droplet and compare it with the numerical results of the GP equation. In Sec. IV, we obtain a formula for the vortex core size and compare it with the numerical solution. We also discuss the corrections to the uniform triangular lattice. In Sec. V, we discuss the possibility of obtaining a vortex lattice with lower filling factors. In Sec. VI, we discuss the experimental parameters required to realize the suggested phenomena and outline future research directions.

II. MODEL AND PARAMETER REGIMES

We consider a weakly interacting binary BEC with equal masses $m_1 = m_2 = m$ and wave functions $\Psi_1(\mathbf{r}) = \Psi_2(\mathbf{r}) = \Psi(\mathbf{r})$, and equal number of atoms $N_1 = N_2 = N/2$. Intracomponent s-wave scattering lengths are also assumed equal and repulsive $a_{11} = a_{22} \equiv a > 0$ but the intercomponent scattering length is negative: $a_{12} < -a$. This gives a slightly attractive MF interaction such that effectively repulsive BMF energy becomes significant for the condensate's mechanical stability [12]. We assume that the density gradient is sufficiently low throughout the condensate such that the local-density approximation (LDA) holds [12,22,23]. The droplet is confined radially with angular frequency $\omega_\perp$ and along the z axis with an angular frequency ω_z. The total energy functional of the mixture is

$$E = \int dV \left\{ \frac{\hbar^2}{2m}|\nabla\Psi|^2 + \frac{1}{2}mw_z^2z^2|\Psi|^2 + \frac{1}{2}mw_\perp^2r^2|\Psi|^2 + \frac{g(1-\alpha_s)}{4}|\Psi|^4 + \frac{8\sqrt{2}}{15\sqrt{\pi}}ga^{3/2}(1+\alpha_s)^{5/2}|\Psi|^5 \right\}, \tag{1}$$

where $\mathbf{r} = (x, y)$ is the position vector, $\alpha_s = |a_{12}|/a$ is the ratio of the scattering lengths, and $g = 4\pi\hbar^2 a/m$ is the coupling constant. The first and second terms in the second line of Eq. (1) are the MF and BMF energies, respectively. Note that the MF energy becomes attractive when α_s becomes slightly greater than 1. In the experiments, α_s can be tuned via Feshbach resonance.

We assume tight confinement in the z direction and integrate the energy functional by assuming a Gaussian wave function $\phi_0(z) = \frac{1}{(\pi a_z)^{1/4}}e^{-z^2/2a_z^2}$, with $a_z = \sqrt{\frac{\hbar}{m\omega_z}}$, i.e., $\Psi(\mathbf{r}, z) = \psi(\mathbf{r})\phi_0(z)$. While tight confinement in the third direction may seem to contrast with the LDA assumption, recent works have shown that the transition from three- to two-dimensional (2D) behavior is smooth [24,25]. The integrated form of the local-energy functional in Eq. (1) is qualitatively similar to the strictly two-dimensional LDA functional where the energy functional has the form $|\Psi|^4 \ln(|\Psi|^2/\sqrt{e})$ [17,18]. They both feature a shallow minimum below zero and a rapid rise after becoming positive. We also expect that integrating out the z axis provides better quantitative agreement with the typical experimental confinement scenarios. In a frame rotating with angular velocity $\boldsymbol{\Omega} = \Omega\hat{e}_z$, minimization of the

functional $E - \Omega L_z$ [26], with L_z being angular momentum, gives the dimensionless extended GP equation scaled with the radial trapping frequency $\omega_\perp$ as

$$\tilde{\mu}\tilde{\psi} = -\tfrac{1}{2}(\tilde{\nabla} - \tilde{\mathbf{\Omega}} \times \tilde{\mathbf{r}})^2\tilde{\psi} + \tfrac{1}{2}\tilde{r}^2(1-\tilde{\Omega}^2)\tilde{\psi} + \gamma_{\rm int}[(1-\alpha_s)|\tilde{\psi}|^2 + \beta_{\rm LHY}|\tilde{\psi}|^3]\tilde{\psi}, \quad (2)$$

where $\tilde{\mathbf{r}} = \mathbf{r}/a_\perp$, $\tilde{\nabla} = a_\perp\nabla$, $\tilde{\psi} = a_\perp\psi$, $\tilde{\Omega} = \Omega/\omega_\perp$. The interaction parameters are $\gamma_{\rm int} \equiv \sqrt{2\pi}\frac{a}{a_z}$ and $\beta_{\rm LHY} \equiv \frac{16\sqrt{2}}{3\sqrt{5}\pi^{3/4}}\frac{a^{3/2}}{a_z^{1/2}a_\perp}(1+\alpha_s)^{5/2}$, where $a_\perp = \sqrt{\frac{\hbar}{m\omega_\perp}}$. Note that in the rapid rotation limit $\tilde{\Omega} \to 1$ the gas is still mechanically stable due to the balance between mean-field attraction and Lee-Huang-Yang (LHY) quantum fluctuations, in stark contrast with regular BECs.

Physical scales in the strictly two-dimensional limit are determined by the oscillator length $a_\perp$, the inter- and intracomponent scattering lengths a_{12} and a, and the total particle number N. The oscillator length $a_\perp$, giving the typical 2D cloud size in the trap, is used as the unit of length. The confinement along z creates an additional length scale a_z, which will be used to tune effective two-dimensional interaction $\gamma_{\rm int} \sim a/a_z$. The ratio of inter-to-intracomponent interaction $\alpha_s = |a_{12}|/a$ controls the attractive mean-field interaction, and the droplet forms when it is larger than 1 yet the gas remains dilute. Last but not least, the dimensionless parameter $\beta_{\rm LHY}$ determines the importance of the Lee-Huang-Yang BMF repulsion compared with the MF attraction. Although the parameters α_s, $\beta_{\rm LHY}$, and $\gamma_{\rm int}$ seem to be interdependent at first sight, each is a unique combination of s-wave scattering and the two oscillator lengths, and we choose to consider them as independent parameters in the following for simplicity.

The limit of dominant interactions over both the kinetic and potential energies is a particularly important regime for droplet physics. In this case, the GP equation in (2) reduces to

$$\tilde{\mu}\tilde{\psi} = \gamma_{\rm int}[(1-\alpha_s)|\tilde{\psi}|^2 + \beta_{\rm LHY}|\tilde{\psi}|^3]\tilde{\psi}. \quad (3)$$

The equilibrium density $n_{\rm min}$ can be found by minimizing the term in the square brackets in (3) with respect to $|\tilde{\psi}|$ as

$$n_{\rm min} = \frac{4(\alpha_s-1)^2}{9\beta_{\rm LHY}^2}, \quad (4)$$

which is the density of a self-trapped droplet. In the "TF droplet" regime, the kinetic energy is negligible and the density is flat if the trap potential is weak. Stronger trap potential squeezes the cloud to the center to minimize the confinement energy, which gives a convex peak at the center that rapidly falls near the surface. Outside the TF regime, which we call the "weak droplet" regime, the kinetic energy is non-negligible compared to the interaction energy, and the wave-function gradient gradually smears the flat-top profile. Here, the droplet is still self-trapped but the density profile has deviations from $n_{\rm min}$ due to the kinetic energy.

To quantify these regimes, we consider a constant density droplet with $\tilde{\psi}(\tilde{r}) = \sqrt{n_{\rm min}}\theta(R_{\rm TF} - \tilde{r})$, where θ is the Heaviside step function. For N particles uniformly filling a circle of radius R, the scaling is obtained as $E_k \sim N/R^2$ for kinetic energy, $E_p \sim NR^2$ for potential energy, $E_{\rm MF} \sim (N/R^2)N$ for MF interaction, and $E_{\rm LHY} \sim (N/R^2)^{3/2}N$ for fluctuations. However, due to the length scale corresponding to density $n_{\rm min}$, the radius and the particle number are not independent.

TABLE I. Different regimes of the rotating confined droplet problem. The conditions in Eqs. (8) and (9) are used to determine the different regimes.

	Strongly confined	Weakly confined
TF droplet	$\frac{1}{\gamma_{\rm int}\lvert\alpha_s-1\rvert N} \ll 1$ $\frac{\beta_{\rm LHY}^4}{\gamma_{\rm int}\lvert\alpha_s-1\rvert^5}N \gtrsim 1$	$\frac{1}{\gamma_{\rm int}\lvert\alpha_s-1\rvert N} \ll 1$ $\frac{\beta_{\rm LHY}^4}{\gamma_{\rm int}\lvert\alpha_s-1\rvert^5}N \ll 1$
Weak droplet	$\frac{1}{\gamma_{\rm int}\lvert\alpha_s-1\rvert N} \approx 1$ $\frac{\beta_{\rm LHY}^4}{\gamma_{\rm int}\lvert\alpha_s-1\rvert^5}N \gtrsim 1$	$\frac{1}{\gamma_{\rm int}\lvert\alpha_s-1\rvert N} \approx 1$ $\frac{\beta_{\rm LHY}^4}{\gamma_{\rm int}\lvert\alpha_s-1\rvert^5}N \ll 1$

Expression $\int n_{\rm min}d^2\tilde{r} = N$ gives the TF radius of the flat-top droplet $R_{\rm TF} = \frac{3\beta_{\rm LHY}}{2\sqrt{\pi}(\alpha_s-1)}\sqrt{N}$ and we find

$$E_{\rm int} = \frac{-14}{135}\frac{\gamma_{\rm int}|\alpha_s-1|^3}{\beta_{\rm LHY}^2}N, \quad (5)$$

$$E_p = \frac{9}{16\pi}\frac{\beta_{\rm LHY}^2}{|\alpha_s-1|^2}N^2, \quad (6)$$

$$E_k = \frac{2\pi}{9}\frac{|\alpha_s-1|^2}{\beta_{\rm LHY}^2}, \quad (7)$$

where $E_{\rm int}$ is the total interaction energy. In the TF regime, the total interaction energy is much larger than the kinetic energy:

$$\frac{E_k}{|E_{\rm int}|} = \frac{30\pi}{14}\frac{1}{\gamma_{\rm int}|\alpha_s-1|N} \ll 1. \quad (8)$$

In the strong confinement regime, the potential energy is larger than the interaction energy:

$$\frac{E_p}{|E_{\rm int}|} = \frac{1215}{224\pi}\frac{\beta_{\rm LHY}^4}{\gamma_{\rm int}|\alpha_s-1|^5}N \gtrsim 1. \quad (9)$$

Since $\gamma_{\rm int}$ independently scales the interaction energy, one can drive the system into the weakly confined TF regime by increasing $\gamma_{\rm int} \propto a/a_z$. Interaction energy (5) and the potential (6) scale with N and N^2, respectively, whereas the kinetic energy (7) has a slower dependence [considering the full GP equation rather than the estimations Eqs. (5)–(7)]. Therefore, the strongly confined TF regime can be achieved by large particle number N. Note that the condition (8) for the TF regime is independent of $\beta_{\rm LHY}$, since both the interaction (5) and kinetic (7) energies scale with $\beta_{\rm LHY}$. The different parameter regimes are summarized in Table I. The strongly confined TF regime, where kinetic energy is negligible but potential energy causes a significant curvature in the equilibrium density, is eventually realized for all parameters if the number of particles is large enough.

III. STRONGLY CONFINED THOMAS-FERMI REGIME

Rotating weakly confined droplets result in either COM motion that preserves the cloud density profile [13,14] or so-called splitting instability that divides the system into smaller fragments [16,17]. Stronger confinement prevents both of these undesirable effects and enables access to rapid rotation limits with stable vortex lattices. In this section, we focus on strongly confined rotating droplets in the TF regime and examine the coarse-grained density profile of the cloud as a function of the rotation frequency $\tilde{\Omega}$.

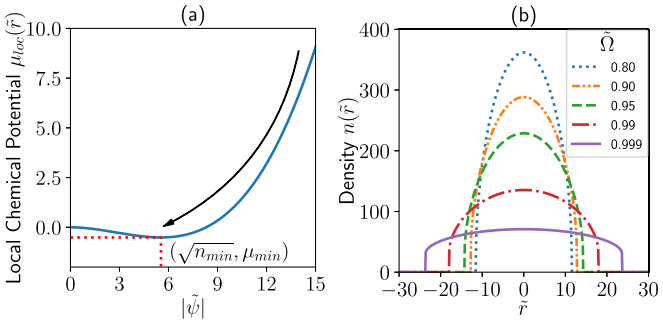

FIG. 1. (a) The local chemical potential $\mu_{\rm loc}(\tilde{r}) = \tilde{\mu} - \frac{1}{2}\tilde{r}^2(1 - \tilde{\Omega}^2)$ in (10) vs $|\tilde{\psi}|$ (blue line). Since $\alpha_s > 1$ and $\beta_{\rm LHY}$ is positive, $\mu_{\rm loc}$ shows a local negative minimum at $|\tilde{\psi}| = \sqrt{n_{\rm min}}$, then monotonically increases with $|\tilde{\psi}|$. The solution to (10) for $\tilde{\mu} > \tilde{\mu}_{\rm min}$ can be found by evaluating $\mu_{\rm loc}(\tilde{r})$ for different $\tilde{r}$, along the curved arrow. The density jumps to zero when the local chemical potential is equal to the minimum value $\mu_{\rm min}$. (b) The analytical solutions of the GP equation (10) of the rotating Bose mixture droplets in the strongly confined TF regime for various $\tilde{\Omega}$. The parameters are $\alpha_s = 1.05$, $\beta_{\rm LHY} = 6 \times 10^{-3}$, $\gamma_{\rm int} = 1, N = 10^5$. The convexity due to the strong confinement flattens and approaches the flat-top profile as $\tilde{\Omega} \to 1$.

When a regular vortex lattice is formed, the kinetic energy of the rotating condensate is nearly equal to the energy of a solid body rotating with angular velocity $\mathbf{\Omega}$. The GP equation governing the coarse-grained density profile is found by neglecting the first term in (2):

$$\tilde{\mu}\tilde{\psi} - \tfrac{1}{2}\tilde{r}^2(1 - \tilde{\Omega}^2)\tilde{\psi} = \gamma_{\rm int}[(1 - \alpha_s)|\tilde{\psi}|^2 + \beta_{\rm LHY}|\tilde{\psi}|^3]\tilde{\psi}, \tag{10}$$

which manifests that the rotation affects the density profile mainly through centrifugal potential. The particles are squeezed toward the center for strong confinement, whereas the centrifugal potential softens the effective trapping frequency $(1 - \tilde{\Omega}^2)$.

As shown in Fig. 1(a), the local chemical potential $\tilde{\mu}_{\rm loc}$ obtained from (10) as a function of $|\tilde{\psi}|$ has negative minimum $\tilde{\mu}_{\rm min}$ at $|\tilde{\psi}| = \sqrt{n_{\rm min}}$, since $\alpha_s > 1$ and $\beta_{\rm LHY} > 0$. Now consider the solution $|\tilde{\psi}|$ of (10) for a given chemical potential $\tilde{\mu} > \tilde{\mu}_{\rm min}$. At the center of the trap $\tilde{r} = 0$, $|\tilde{\psi}|$ takes its maximum value. As $\tilde{r}$ increases, the value of $|\tilde{\psi}|$ follows the path shown by the curved arrow in Fig. 1(a). For the radial position $\tilde{r} = R_0$ at which $|\tilde{\psi}(R_0)| = \sqrt{n_{\rm min}}$, the local chemical potential $\tilde{\mu} - \frac{1}{2}\tilde{r}^2(1 - \tilde{\Omega}^2)$ reaches its minimum, and then $|\tilde{\psi}(\tilde{r})|$ abruptly falls to zero for $\tilde{r} > R_0$. We solve the cubic equation analytically as shown in the Appendix. The solutions of Eq. (10) for different rotation frequencies $\tilde{\Omega}$ are shown in Fig. 1(b), which demonstrate that the cloud flattens as the rotation frequency approaches the limit $\tilde{\Omega} \to 1$.

We verify the above qualitative description by solving the nonlinear GP equation (2) fully numerically in the strongly confined TF regime for the rapid rotations. We find the ground state in the rotating frame by the imaginary time evolution iterated by the split-step Fourier method [27,28]. We consider a typical choice of strongly confined TF regime parameters: $\alpha_s = 1.05$, $\beta_{\rm LHY} = 6 \times 10^{-3}$, $\gamma_{\rm int} = 1$, and $N = 10^5$. This choice gives $\frac{E_k}{|E_{\rm int}|} = 1.37 \times 10^{-4}$, $\frac{E_p}{|E_{\rm int}|} = 2.3 \times 10^3$, $n_{\rm min} \approx 30$, and TF radius $R_{\rm TF} \approx 32$. We tested the convergence of the numerical routine by using random, Gaussian, and Jacobi-theta initial wave functions [10]. Each resulted in almost identical density profiles and locally triangular vortex lattices with occasional dislocation defects. The displayed results in Fig. 2 are for Jacobi-theta function initial conditions, which have a perfectly periodic vortex lattice with a single vortex per hexagonal unit cell. This choice accelerates the convergence to minimum energy considerably and prevents unwanted dislocations in the lattice. The lower panel of Fig. 2 shows the density profiles of the cloud, which follows the solutions of the TF equation (10) (solid lines) with remarkable accuracy. With increasing rotation, the peak density at the center decreases, and the overall profile flattens, whereas the kinetic energy makes a marginal influence by smoothing the jump at the edge of the cloud.

It is important to compare the coarse-grained properties of the rapidly rotating droplet with the vortex lattices in the usual repulsive BEC experiments. In ordinary BECs, the TF profile always remains an inverted parabola, and its radius increases with increasing rotation. For droplets, there is a finite density jump at the surface and the functional form smoothly changes from a high curvature profile to a flat profile with increasing density. Notice that the cloud size of the rotating droplet for $\tilde{\Omega} = 0.8$ and 0.97 is not substantially different in Fig. 2. In fact, as $\tilde{\Omega}$ increases towards 1, the cloud radius converges to the nonrotating TF radius $R_{\rm TF}$, whereas it diverges for the repulsive BECs in both TF and LLL regimes [9,20,21,29]. This is a remnant of the celebrated self-trapping property of the droplets, where in this case the fast rotation diminishes the external trapping potential but the competition between MF attraction and LHY repulsion constrains the increase of the cloud radius. More concretely, for the repulsive BEC in TF and LLL regimes, the cloud radius scales with $R(\tilde{\Omega})/R(0) = (1 - \tilde{\Omega}^2)^{-3/10}$ and $(1 - \tilde{\Omega})^{-1/4}$, respectively [6]. For the TF droplet, we calculate the radius for various $\tilde{\Omega}$ from (10) in the Appendix, and also estimate it from the full numerical solutions of Eq. (2) as shown in Fig. 3. One can see that the droplet radius remains much smaller than the regular BEC cloud radius, even in the extremely rapid rotation limit.

Most of the rotating BEC experiments were limited in the upper rotation frequencies due to the imperfections in the harmonic trap [30]. These imperfections are harder to control away from the trap's center, and as the cloud radius gets larger they dissipate angular momentum. We believe that the small change in the size of the droplet with rotation can make the rapid rotation limit easier to reach.

IV. PROPERTIES OF THE VORTEX LATTICE

The numerical results shown in Fig. 2 reveal that the vortex core sizes are visibly different at the edge of the droplet compared with the center (see Fig. 4 for a comparison). This sharply contrasts with the repulsive BECs where the cores in the vortex lattices are almost uniform in size throughout the system [31]. In this section, we focus on the core sizes

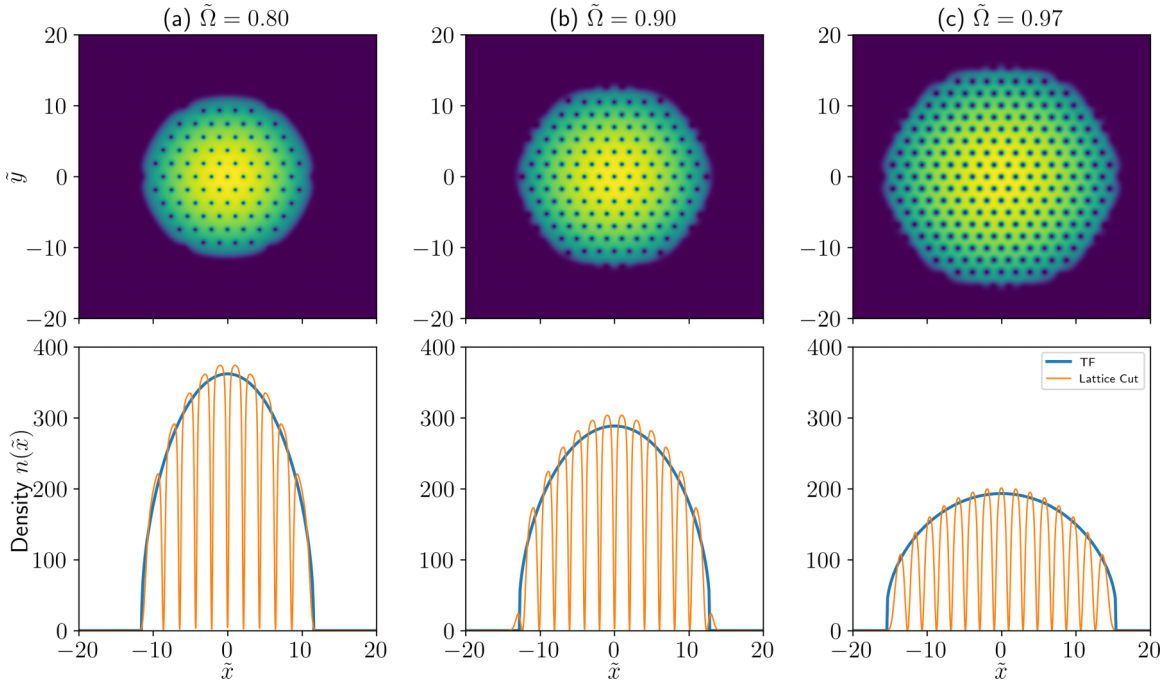

FIG. 2. The numerical solutions of the GP equation (2) of the rotating Bose mixture droplets for the parameters $\alpha_s = 1.05$, $\beta_{\rm LHY} = 6 \times 10^{-3}$, $\gamma_{\rm int} = 1$, $N = 10^5$, and (a) $\tilde{\Omega} = 0.80$, (b) $\tilde{\Omega} = 0.90$, and (c) $\tilde{\Omega} = 0.97$. Upper panel: 2D density profiles of the vortex lattices. Lower panel: Density profile of the vortex lattices along the x axis (orange lines) and the rotating TF solution of the GP equation (10) (blue lines). The scaled lengths are $\tilde{x} \equiv x/a_\perp$ and $\tilde{y} \equiv y/a_\perp$.

in the rapidly rotating TF droplet, and also the related lattice distortions previously known in the study of nonuniform superfluids, to better understand these observations.

Substituting the chemical potential $\tilde{\mu} = (1 - \alpha_s)n_0 + \beta_{\rm LHY} n_0^{3/2}$ corresponding to a uniform bulk density n_0 in Eq. (3), one can obtain

$$\tfrac{1}{2}\tilde{\nabla}^2\tilde{\psi} = (1 - \alpha_s)(|\tilde{\psi}|^2 - n_0)\tilde{\psi} + \beta_{\rm LHY}\left(|\tilde{\psi}|^3 - n_0^{3/2}\right)\tilde{\psi}. \tag{11}$$

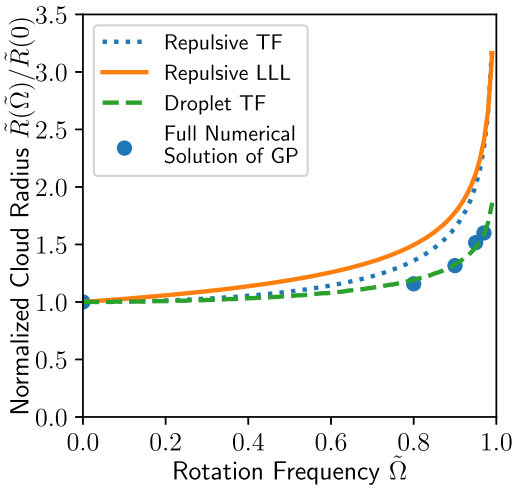

FIG. 3. The comparison of the radius of the condensates for the rotation frequency $\tilde{\Omega} \in [0, 1]$: Repulsive BEC in the TF regime (dotted), repulsive BEC in the LLL regime (solid), and droplet in the TF regime (dashed). The scattered data present the radius of the full numerical solutions of GP (2). The droplet radius converges to a finite value as $\tilde{\Omega} \to 1$, contrary to the diverging behavior of the repulsive BECs.

First, we obtain an analytical formula for the coherence length as follows. We consider a semi-infinite condensate filling the right half plane near an impenetrable surface to reduce this equation to a one-dimensional (1D) form. Multiplying both sides of Eq. (11) by $\partial\tilde{\psi}/\partial\tilde{x}$ and assuming a positive real wave function $\tilde{\psi}(\tilde{x}) \geqslant 0$ for $\tilde{x} \geqslant 0$, we obtain

$$\frac{1}{2}\frac{\partial}{\partial\tilde{x}}\left(\frac{\partial\tilde{\psi}}{\partial\tilde{x}}\right)^2 - \frac{\partial V}{\partial\tilde{\psi}}\frac{\partial\tilde{\psi}}{\partial\tilde{x}} = 0, \tag{12}$$

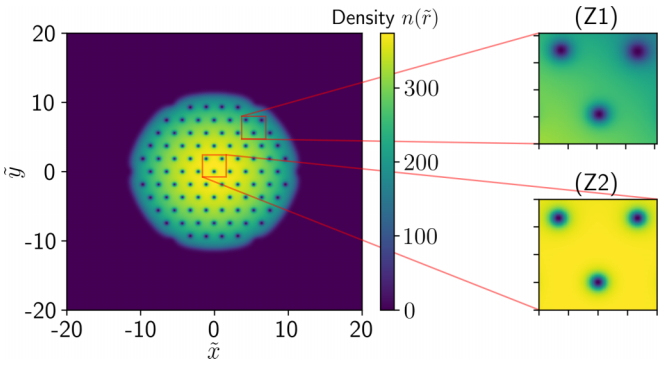

FIG. 4. Density profile of the vortex lattice with $\tilde{\Omega} = 0.8$ in Fig. 2(a). The insets show the 2D zooms of equal areas in the vortex lattice near the edge (Z1) and the center (Z2) of the droplet. The core size is larger, and the vortex unit cell area decreases near the edge.

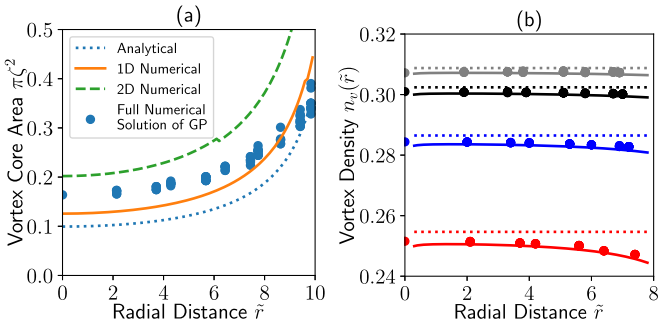

FIG. 5. (a) The vortex core area estimates by numerical solutions of 1D (solid line) and 2D (dashed line) healing length equation (11), analytical approximation (14) (dotted line), and the full numerical solution of GP (2) for (filled points) $\tilde{\Omega} = 0.8$. The density levels n_0 for the numerical and analytical solutions to (11) and (14) are taken from the strongly confined TF droplet equation (10). The difference in the core size along the TF droplet is more tractable than the repulsive BECs. (b) The vortex density of the rotating TF droplet calculated up to the first order in (15) for $\tilde{\Omega} = 0.80$ (gray), $\tilde{\Omega} = 0.90$ (black), $\tilde{\Omega} = 0.95$ (blue), and $\tilde{\Omega} = 0.97$ (red). The dotted lines represent the uniform vortex densities $n_{v0} = \tilde{\Omega}/\pi$. The scattered data show the vortex density computed on the full numerical solution of GP (2) in Fig. 2, whereas the solid lines are the solutions to (15). The vortex density closely follows the uniform limit with an agreement on the corrections.

where

$$V[\tilde{\psi}] = (1-\alpha_s)\left(\tfrac{1}{2}\tilde{\psi}^4 - n_0\tilde{\psi}^2\right) + \beta_{\rm LHY}\left(\tfrac{2}{5}\tilde{\psi}^5 - n_0^{3/2}\tilde{\psi}^2\right). \tag{13}$$

This shows that $\frac{1}{2}(\partial\tilde{\psi}/\partial\tilde{x})^2 - V[\tilde{\psi}]$ is a constant of motion. Evaluating this constant for the limits $\tilde{x} \to 0$ and ∞, where $\lim_{\tilde{x}\to 0,\infty}\tilde{\psi} = 0, \sqrt{n_0}$, gives the healing length scale of the condensate $\zeta \approx \sqrt{n_0}/\lim_{\tilde{x}\to 0}(\frac{\partial\psi}{\partial\tilde{x}})$:

$$\zeta = \frac{1}{\sqrt{\frac{6\gamma_{\rm int}\beta_{\rm LHY}}{5} n_0\left(n_0^{1/2} - n_c^{1/2}\right)}}, \tag{14}$$

where $n_c = \frac{25(\alpha_s-1)^2}{36\beta_{\rm LHY}^2}$ is the droplet density scale $n_{\rm min}$ up to a numerical factor of order 1. The analytical approximation fails for densities n_0 below n_c, signaling the splitting instability. For a better comparison, we also calculate the coherence length by numerically solving Eq. (11) in 1D and 2D geometries with the same boundary conditions.

Note that either solution estimates the core size using a constant density n_0 in the bulk, whereas the vortex lattice density follows the TF density profile $n(\tilde{r})$, which is the solution of Eq. (10). Therefore, we derive the radial dependence of the core size $\zeta(\tilde{r})$ by replacing n_0 with $n(\tilde{r})$. We also extract independent estimations from the full numerical solutions of the GP equation (2). As shown in Fig. 5, both the numerical estimates and the analytical result agree with the full numerical solution of GP (2). The core size at the center of the droplet is smaller with respect to the surface of the cloud since the density of the condensate decreases towards the edge.

In the rapidly rotating repulsive BECs in the TF regime, the core size $\zeta \propto \sqrt{\tilde{\Omega}/2gn_0}$ [6] and the TF density profile is inverse parabola. For the TF droplet, the core size scales with the form given in Eq. (14), and the density is still finite $n_{\rm min}$ near the surface. The density scale n_c at the denominator gives a greater sensitivity of the core size to the density changes in the condensate. Furthermore, the finite density near the surface makes the vortices near the surface more visible compared to the surface of the inverse-parabola profile. We expect that the differences in the vortex cores at the center and near the surface of the condensate should be more observable for the TF droplets with respect to the repulsive BECs.

Inhomogeneous superfluid density causes deviations in the local lattice constant, and the vortex density of an infinite uniform lattice given by Feynman relation $n_{v0} = \tilde{\Omega}/\pi$ changes slightly. For rotating droplets, we numerically calculate this local change in the triangular lattice using image processing tools on the full numerical solution of the GP (2) and observe similar deviations. To estimate such changes in the vortex density, we follow the approach in Ref. [32]:

$$n_v(\tilde{r}) = \frac{\tilde{\Omega}}{\pi} + \frac{1}{8\pi}\tilde{\nabla}\cdot\left\{\frac{1}{n(\tilde{r})}\tilde{\nabla}\left[n(\tilde{r})\ln\left(\frac{e}{\pi\zeta^2(\tilde{r})n_v(\tilde{r})}\right)\right]\right\}, \tag{15}$$

where $n_v(\tilde{\Omega})$ is the vortex density, $n(\tilde{r})$ is the condensate density, and $\zeta(\tilde{r})$ is the coherence length. The first term in (15) is the uniform vortex density n_{v0} in dimensionless form, and the second term is the aforementioned small correction. We find the value of Eq. (15) numerically in the strongly confined TF droplet regime using the analytical superfluid density $n(\tilde{r})$ calculated in Eq. (A1), and the coherence length $\zeta(\tilde{r})$ calculated from (14) by replacing n_0 with $n(\tilde{r})$. As the system is still well described by a single collective wave function, we expect the deviation between the superfluid density and the particle density to be small. We compare the results with the vortex density profile of the full numerical GP solution for different values of $\tilde{\Omega}$ in Fig. 5(b).

The deviations from the uniform vortex density are due to the gradient of the superfluid density. Since the TF density profile becomes more flat as the rotation $\tilde{\Omega}$ increases, the deviations from the uniform vortex density are greater for the slower rotations. Deviations become larger close to the edge of the droplet due to the convex profile. However, as $\tilde{\Omega} \to 1$, the density profile approaches a flat-top shape, and the vortex density gets close to the uniform vortex density throughout the condensate. We expect an almost perfect triangular lattice for the highest rapid rotation rates, unlike the radially distorted vortex lattice in the repulsive TF BECs [32].

V. VORTEX LATTICES WITH LOW FILLING FACTORS

Reaching the strongly correlated regime in rapidly rotating ultracold gases to mimic the physics of electrons in quantum Hall systems is one of the major challenges in atomic, molecular, and optical physics [30,33]. Recently, the realization of fractional quantum Hall states is reported for photons and Bose gases but only with few particles [34,35]. These experiments are far from simulating the full many-body physics at the mesoscopic scale, where some emergent properties, such as interaction-induced incompressibility, can be observed. Rapid rotation, which is the analog of the strong

magnetic field in a neutral cold atomic gas, effectively reduces the confining potential for the repulsive BECs in a harmonic trap. As $\tilde{\Omega}$ increases, the condensate enters the MF LLL regime, where intervortex spacing becomes comparable to vortex core size. For a two-dimensional condensate uniform over a length Z in the transverse direction, the cloud size is given by $R_0 = (\frac{8Nad_\perp^4}{Z(1-\tilde{\Omega})})^{1/4}$ in the MF LLL regime [6], which diverges as $\tilde{\Omega} \to 1$. As the interparticle distance approaches the intervortex spacing, the quantum fluctuations become relevant, and the GP MF description becomes insufficient [30]. One may still ask, however, whether some preliminary hints of many-body correlations emerge from the GP approach before it breaks down completely.

The importance of correlations is characterized by the filling factor $\nu = N/N_v$, where N and N_v are particle and vortex numbers, respectively [36,37]. For $\nu \approx 5$–10, the quantum fluctuations are expected to melt the vortex lattice and drive the system into a fractional quantum Hall phase [38]. In the MF LLL regime, the number of vortices is given by $N_v \approx R_0^2/a_\perp^2$ and the corresponding filling factor is [6,30]

$$\nu \equiv \frac{N}{N_v} = \sqrt{\frac{Z(1-\tilde{\Omega})N}{8a}}. \tag{16}$$

For typical values of $Z/a \approx 100$, $N \approx 1000$, rotation rates $\tilde{\Omega} > 0.99$ are needed to achieve $\nu \approx 5$. For such high values of $\tilde{\Omega}$, the cloud size is much larger than the nonrotating condensate size.

As discussed in the previous sections, a rotating droplet's size changes only fractionally in the strongly confined TF limit, hinting at the possibility of achieving lower filling factors. Rotating droplets approach a flat-top particle density $n_{\min}$ whereas the approximate vortex density is $n_{v0} = \tilde{\Omega}/\pi$. Assuming that the radius is close to the flat-top TF radius $R_{\rm TF}$, the filling factor of the rotating droplet becomes

$$\nu = \frac{N}{\pi R_{\rm TF}^2 n_v} = \frac{\pi n_{\min}}{\tilde{\Omega}}. \tag{17}$$

This shows that a lower filling factor can be achieved via smaller droplet density $n_{\min}$. As an example, we consider the parameters $N = 500$, $\alpha_s = 1.25$, $\beta_{\rm LHY} = 0.15$, $\gamma_{\rm int} = 10$, which theoretically result in a strongly confined TF droplet with $n_{\min} \approx 1.2$, $R_{\rm TF} = 11.5$. For $\tilde{\Omega} = 0.99$, the filling factor is close to $\nu \approx 3.8$. The full numerical solution of the GP equation (2) is obtained for these parameters, and the 2D density profile of the vortex lattice is shown in Fig. 6, which displays about 70–80 vortices giving a filling factor $\nu \approx 6.25$. The difference between the numerical result and the theoretical expectation is due to the fact that the density profile is far from the flat-top regime for this parameter choice.

The vortex lattice in a droplet has two distinct instabilities in the rapid rotation limit. At low filling factors, quantum melting due to fluctuations destroys the vortex lattice, paving the way for the strongly correlated phases. The other possibility is that as the droplet density becomes flatter a large portion of the density approaches $n_{\min}$ and vortex core sizes exceed the intervortex spacing. This is the same mechanism of splitting as seen in weakly trapped droplets. As our above example shows, it is possible to get into the low filling factor regime while avoiding the weakly trapped regime. We believe

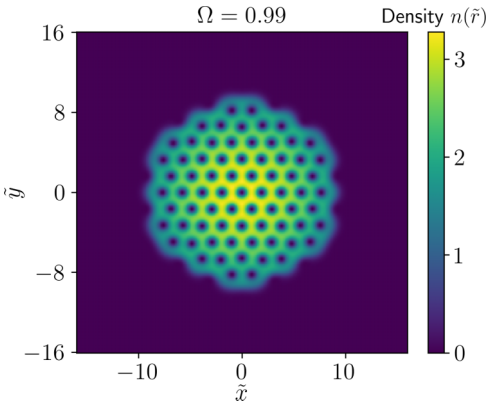

FIG. 6. The vortex lattice of a rotating strongly confined droplet with a low filling factor. There are approximately 80 vortices for particle number $N = 500$, i.e., $\nu \approx 6.25$. The parameters are $\alpha_s = 1.25$, $\beta_{\rm LHY} = 0.15$, $\gamma_{\rm int} = 10$, and $\tilde{\Omega} = 0.99$.

that the tunability of the equilibrium density, as well as the weak size change under rapid rotation, make droplets ideal systems to probe low filling factor physics.

VI. DISCUSSION, EXPERIMENTAL REALIZATION, AND CONCLUSION

The standard approach of using a modified GP equation to describe the system can break down in two ways. On one hand, condensate wave function Ψ can be destroyed in a strongly correlated phase, giving rise to a many-body phase without a local order parameter. On the other hand, the vortex lattice can strongly modify fluctuations so that the LDA assumption is violated even before the onset of the strongly correlated regime. We do not expect the GP equation to describe the system near the transition quantitatively. However, we believe that our calculations show that much lower filling factors than what has been observed are possible with droplets.

There are several intriguing questions that require further research. To achieve an analog of electronic phases under ultrastrong magnetic fields, it becomes essential to import larger angular momenta into the system, resulting in lower filling factors. The central challenge in cold atom experiments, as discussed earlier, is the cancellation of trapping potential due to the centrifugal potential. Our paper reveals that droplets can overcome this challenge through self-trapping, a consequence of the balance between attractive MF interactions and effectively repulsive LHY quantum fluctuations. It is important to note that a low filling factor does not necessarily imply strongly correlated physics for a droplet, as the GP formalism is still a mean-field approach. Similarly, whether a rapidly rotating quantum droplet can be described within the LLL regime needs more investigation. The traditional condition for the LLL regime, $\mu \approx gn_0 \ll 2\hbar\omega_\perp$, is not applicable since the chemical potential of the self-trapped droplet is negative. Consequently, the stabilization of the cloud by quantum fluctuations and whether this stabilization mechanism still exists in the LLL regime should be explored.

The Bose mixture droplets without any trap are experimentally realized by several groups [39–42]. Similar

to our assumptions in this paper, the validity of the LDA treatment of the MF and LHY terms, and the physics of vortices and vortex lattices, are theoretically established in the recent work on dipolar droplets [43–48]. Furthermore, the vortex arrays are experimentally obtained in rotating dipolar condensates [49,50], in which the extended GP equation with the LDA is numerically benchmarked. It is promising for our proposal that the extended GP approach shows good agreement between the numerical estimates and the experimental results [49,50].

Let us consider the feasibility of an experiment to realize the vortex lattices in the Bose mixture droplets. The nondimensional parameters which control the different regimes of the problem are $\alpha_s = \frac{|a_{12}|}{a}$, $\gamma_{\rm int} \equiv \sqrt{2\pi}\frac{a}{a_z}$, and $\beta_{\rm LHY} \equiv \frac{16\sqrt{2}}{3\sqrt{5}\pi^{3/4}}\frac{a^{3/2}}{a_z^{1/2}a_\perp}(1+\alpha_s)^{5/2}$. To obtain results close to the parameter choice of this paper, we consider a Bose mixture of hypothetical atoms with 39 atomic mass units in states $|1,0\rangle$ and $|1,-1\rangle$ with total particle number $N = 10^5$. The scattering lengths are $a = 60a_0$ and $a_{12} = -63a_0$, where a_0 is the Bohr radius. The radial and vertical trap frequencies are $\omega_\perp/2\pi = 505$ Hz and $\omega_z/2\pi = 410$ Hz. The corresponding trap length scales are $a_z \approx 800$ nm and $a_\perp \approx 715$ nm. These conditions yield 2.8–4.5-μm size of the rotating droplet for $\tilde{\Omega} \approx 0.80$–$0.97$. For the case $a_{11} \neq a_{22}$, the qualitative behavior of the rotating droplets should stay the same as long as $\delta a \propto a_{12} + \sqrt{a_{11}a_{22}} < 0$. However, the MF and LHY energies should be revised accordingly. We believe that this generalization is not necessary to explain the fundamental arguments of this paper, but may be left for future work. Furthermore, the three-body losses can be suppressed by either lowering the equilibrium density $n_{\rm min}$ or directly cooling into the vortex lattice state [51]. Note that this particular choice of parameters is only illustrative. Similar phenomena can be observed in a wide regime of parameters.

In summary, we find that a triangular vortex lattice is obtained for a strongly confined TF droplet under rapid rotation. The overall density profile of the cloud follows the TF form even in the presence of the lattice. We investigated the lattice's vortex core size and vortex density and obtained good agreement between analytical and numerical results. The condensate size does not diverge at extreme rapid rotation $\tilde{\Omega} \to 1$, due to self-trapping. This behavior can provide greater experimental feasibility to reach rapid rotation. Furthermore, the lattices with low filling factors can be achieved by tuning the droplet density. A more detailed investigation of the rapidly rotating droplet phase is required to determine if the fluctuation-induced stability mechanism extends to noncondensed bosonic phases such as the fractional quantum Hall states. Additionally, this research can also be carried out for the heteronuclear droplets, in which the three-body losses are suppressed more effectively [41].

Note added. Recently, we became aware of a paper that studies the rotating Bose mixture droplets at the limit $\tilde{\Omega} = 1$ [52].

ACKNOWLEDGMENT

This work is supported by TUBITAK 2236 cofunded Brain Circulation Scheme 2 (CoCirculation2) Project No. 120C066 (A.K.). U.T. is partially supported by TUBTAK 2210 fellowship.

APPENDIX: ANALYTICAL SOLUTION OF THE CUBIC TF EQUATION

The cubic equation $ax^3 + bx^2 + cx + d = 0$ can be reduced into the depressed form $t^3 + pt + q = 0$ with the change of variables $t = x + \frac{b}{3a}$, where $p = \frac{3ac-b^2}{3a^2}$ and $q = \frac{2b^3-9abc+27a^2d}{27a^3}$. The real solution to the problem can be found in the trigonometric form. Now consider the GP equation (10) for the strongly confined TF droplet, which is a cubic equation with $c = 0$. Apply the change of variables $t = |\tilde{\psi}| + \frac{1-\alpha_s}{\beta_{\rm LHY}}$. The trigonometric solution becomes

$$|\tilde{\psi}(\tilde{r} \leqslant R_{\rm TF})| = \frac{2(\alpha_s-1)}{3\beta_{\rm LHY}}\left\{\frac{1}{2} + \cos\left[\frac{1}{3}\arccos \times\left(1 + \frac{27\beta_{\rm LHY}^2\mu_{\rm loc}(\tilde{r})}{2\gamma_{\rm int}(\alpha_s-1)^3}\right)\right]\right\}, \tag{A1}$$

where the local chemical potential $\mu_{\rm loc}(\tilde{r}) = \mu - \frac{\tilde{r}^2}{2}(1-\tilde{\Omega}^2)$ and $R_{\rm TF}$ is the TF radius of the strongly confined TF droplet, where $|\tilde{\psi}(\tilde{R}_{\rm TF})| = \sqrt{n_{\rm min}}$. We calculate $R_{\rm TF}$, where the density falls rapidly, by using $|\tilde{\psi}(\tilde{R}_{\rm TF})| = \frac{2(\alpha_s-1)}{3\beta_{\rm LHY}}$:

$$R_{\rm TF} = \sqrt{\left(\mu + \frac{4\gamma_{\rm int}(\alpha_s-1)^3}{27\beta_{\rm LHY}^2}\right)\frac{2}{1-\tilde{\Omega}^2}} = \sqrt{\frac{2(\mu-\mu_{\rm min})}{1-\tilde{\Omega}^2}}, \tag{A2}$$

where $\mu_{\rm min} = -\frac{4\gamma_{\rm int}(\alpha_s-1)^3}{27\beta_{\rm LHY}^2}$ is the chemical potential of the flat-top droplet. Consider the limit $\tilde{\Omega} \to 1$, in which the external trap is effectively removed by the centrifugal effect, and the droplet approaches the flat-top profile. Hence, the divergence of the droplet radius is prevented as $\lim_{\tilde{\Omega}\to 1}\mu = \mu_{\rm min}$. In fact, one should recover the flat-top radius $R_{\rm TF} = \frac{3\beta_{\rm LHY}}{2\sqrt{\pi}(\alpha_s-1)}\sqrt{N}$ at the limit $\tilde{\Omega} \to 1$.

[1] C. J. Pethick and H. Smith, *Bose-Einstein Condensation in Dilute Gases* (Cambridge University, New York, 2008).

[2] L. Pitaevskii and S. Stringari, *Bose-Einstein Condensation and Superfluidity*, International Series of Monographs on Physics, Vol. 164 (Oxford University, New York, 2016).

[3] K. W. Madison, F. Chevy, W. Wohlleben, and J. Dalibard, Vortex Formation in a Stirred Bose-Einstein Condensate, Phys. Rev. Lett. **84**, 806 (2000).

[4] M. R. Matthews, B. P. Anderson, P. C. Haljan, D. S. Hall, C. E. Wieman, and E. A. Cornell, Vortices in a Bose-Einstein Condensate, Phys. Rev. Lett. **83**, 2498 (1999).

[5] J. R. Abo-Shaeer, C. Raman, J. M. Vogels, and W. Ketterle, Observation of vortex lattices in Bose-Einstein condensates, Science **292**, 476 (2001).

[6] A. L. Fetter, Rotating trapped Bose-Einstein condensates, Rev. Mod. Phys. **81**, 647 (2009).

[7] G. M. Kavoulakis, A. D. Jackson, and G. Baym, Rotating Bose-Einstein condensates with attractive interactions, Phys. Rev. A **70**, 043603 (2004).

[8] K. Kasamatsu, M. Tsubota, and M. Ueda, Vortices in multicomponent Bose-Einstein condensates, Int. J. Mod. Phys. B **19**, 1835 (2005).

[9] T.-L. Ho, Bose-Einstein Condensates with Large Number of Vortices, Phys. Rev. Lett. **87**, 060403 (2001).

[10] E. J. Mueller and T.-L. Ho, Two-Component Bose-Einstein Condensates with a Large Number of Vortices, Phys. Rev. Lett. **88**, 180403 (2002).

[11] A. Chaika, A. Richaud, and A. Yakimenko, Making ghost vortices visible in two-component Bose-Einstein condensates, Phys. Rev. Res. **5**, 023109 (2023).

[12] D. S. Petrov, Quantum Mechanical Stabilization of a Collapsing Bose-Bose Mixture, Phys. Rev. Lett. **115**, 155302 (2015).

[13] S. Nikolaou, G. Kavoulakis, and M. Ogren, Novel superfluid states in rotating quantum droplets confined in a harmonic potential, arXiv:2305.09422.

[14] P. Examilioti and G. Kavoulakis, Ground state and rotational properties of two-dimensional self-bound quantum droplets, J. Phys. B **53**, 175301 (2020).

[15] X. Jiang, Y. Zeng, Y. Ji, B. Liu, X. Qin, and Y. Li, Vortex formation and quench dynamics of rotating quantum droplets, Chaos, Solitons Fractals **161**, 112368 (2022).

[16] Y. Li, Z. Chen, Z. Luo, C. Huang, H. Tan, W. Pang, and B. A. Malomed, Two-dimensional vortex quantum droplets, Phys. Rev. A **98**, 063602 (2018).

[17] Y. V. Kartashov, B. A. Malomed, L. Tarruell, and L. Torner, Three-dimensional droplets of swirling superfluids, Phys. Rev. A **98**, 013612 (2018).

[18] M. N. Tengstrand, P. Stürmer, E. O. Karabulut, and S. M. Reimann, Rotating Binary Bose-Einstein Condensates and Vortex Clusters in Quantum Droplets, Phys. Rev. Lett. **123**, 160405 (2019).

[19] S. R. Otajonov, E. N. Tsoy, and F. K. Abdullaev, Variational approximation for two-dimensional quantum droplets, Phys. Rev. E **102**, 062217 (2020).

[20] V. Schweikhard, I. Coddington, P. Engels, V. P. Mogendorff, and E. A. Cornell, Rapidly Rotating Bose-Einstein Condensates in and near the Lowest Landau Level, Phys. Rev. Lett. **92**, 040404 (2004).

[21] V. Bretin, S. Stock, Y. Seurin, and J. Dalibard, Fast Rotation of a Bose-Einstein Condensate, Phys. Rev. Lett. **92**, 050403 (2004).

[22] F. Wächtler and L. Santos, Ground-state properties and elementary excitations of quantum droplets in dipolar Bose-Einstein condensates, Phys. Rev. A **94**, 043618 (2016).

[23] F. Ancilotto, M. Barranco, M. Guilleumas, and M. Pi, Self-bound ultradilute Bose mixtures within local density approximation, Phys. Rev. A **98**, 053623 (2018).

[24] T. Ilg, J. Kumlin, L. Santos, D. S. Petrov, and H. P. Büchler, Dimensional crossover for the beyond-mean-field correction in Bose gases, Phys. Rev. A **98**, 051604(R) (2018).

[25] P. Zin, M. Pylak, and M. Gajda, Self-consistent description of Bose-Bose droplets: Harmonically trapped quasi-two-dimensional droplets, Phys. Rev. A **106**, 013320 (2022).

[26] E. Lifshitz and L. D. Landau, Statistical Physics Part 2: Theory of the Condensed State, *Course of Theoretical Physics Vol. 9* (Pergamon, London, 1980).

[27] W. Bao, Q. Du, and Y. Zhang, Dynamics of rotating Bose-Einstein condensates and its efficient and accurate numerical computation, SIAM J. Appl. Math. **66**, 758 (2006).

[28] J. Javanainen and J. Ruostekoski, Symbolic calculation in development of algorithms: Split-step methods for the Gross–Pitaevskii equation, J. Phys. A **39**, L179 (2006).

[29] P. Rosenbusch, D. S. Petrov, S. Sinha, F. Chevy, V. Bretin, Y. Castin, G. Shlyapnikov, and J. Dalibard, Critical Rotation of a Harmonically Trapped Bose Gas, Phys. Rev. Lett. **88**, 250403 (2002).

[30] N. R. Cooper, Rapidly rotating atomic gases, Adv. Phys. **57**, 539 (2008).

[31] M.-O. Mewes, M. R. Andrews, N. J. van Druten, D. M. Kurn, D. S. Durfee, C. G. Townsend, and W. Ketterle, Collective Excitations of a Bose-Einstein Condensate in a Magnetic Trap, Phys. Rev. Lett. **77**, 988 (1996).

[32] D. E. Sheehy and L. Radzihovsky, Vortex lattice inhomogeneity in spatially inhomogeneous superfluids, Phys. Rev. A **70**, 051602(R) (2004).

[33] S. Viefers, Quantum Hall physics in rotating Bose-Einstein condensates, J. Phys.: Condens. Matter **20**, 123202 (2008).

[34] L. W. Clark, N. Schine, C. Baum, N. Jia, and J. Simon, Observation of Laughlin states made of light, Nature (London) **582**, 41 (2020).

[35] J. Léonard, S. Kim, J. Kwan, P. Segura, F. Grusdt, C. Repellin, N. Goldman, and M. Greiner, Realization of a fractional quantum Hall state with ultracold atoms, Nature (London) **619**, 495 (2023).

[36] N. K. Wilkin and J. M. F. Gunn, Condensation of "Composite Bosons" in a Rotating BEC, Phys. Rev. Lett. **84**, 6 (2000).

[37] N. R. Cooper, N. K. Wilkin, and J. M. F. Gunn, Quantum Phases of Vortices in Rotating Bose-Einstein Condensates, Phys. Rev. Lett. **87**, 120405 (2001).

[38] J. Sinova, C. B. Hanna, and A. H. MacDonald, Quantum Melting and Absence of Bose-Einstein Condensation in Two-Dimensional Vortex Matter, Phys. Rev. Lett. **89**, 030403 (2002).

[39] C. R. Cabrera, L. Tanzi, J. Sanz, B. Naylor, P. Thomas, P. Cheiney, and L. Tarruell, Quantum liquid droplets in a mixture of Bose-Einstein condensates, Science **359**, 301 (2018).

[40] G. Semeghini, G. Ferioli, L. Masi, C. Mazzinghi, L. Wolswijk, F. Minardi, M. Modugno, G. Modugno, M. Inguscio, and M. Fattori, Self-Bound Quantum Droplets of Atomic Mixtures in Free Space, Phys. Rev. Lett. **120**, 235301 (2018).

[41] C. D'Errico, A. Burchianti, M. Prevedelli, L. Salasnich, F. Ancilotto, M. Modugno, F. Minardi, and C. Fort, Observation of quantum droplets in a heteronuclear bosonic mixture, Phys. Rev. Res. **1**, 033155 (2019).

[42] T. G. Skov, M. G. Skou, N. B. Jørgensen, and J. J. Arlt, Observation of a Lee-Huang-Yang Fluid, Phys. Rev. Lett. **126**, 230404 (2021).

[43] A. Cidrim, F. E. A. dos Santos, E. A. L. Henn, and T. Macrì, Vortices in self-bound dipolar droplets, Phys. Rev. A **98**, 023618 (2018).

[44] S. B. Prasad, T. Bland, B. C. Mulkerin, N. G. Parker, and A. M. Martin, Vortex lattice formation in dipolar Bose-Einstein condensates via rotation of the polarization, Phys. Rev. A **100**, 023625 (2019).

[45] A. Gallemí, S. M. Roccuzzo, S. Stringari, and A. Recati, Quantized vortices in dipolar supersolid Bose-

Einstein-condensed gases, Phys. Rev. A **102**, 023322 (2020).

[46] F. Ancilotto, M. Barranco, M. Pi, and L. Reatto, Vortex properties in the extended supersolid phase of dipolar Bose-Einstein condensates, Phys. Rev. A **103**, 033314 (2021).

[47] A. Gallemí and L. Santos, Superfluid properties of a honeycomb dipolar supersolid, Phys. Rev. A **106**, 063301 (2022).

[48] T. Bland, E. Poli, C. Politi, L. Klaus, M. A. Norcia, F. Ferlaino, L. Santos, and R. N. Bisset, Two-Dimensional Supersolid Formation in Dipolar Condensates, Phys. Rev. Lett. **128**, 195302 (2022).

[49] L. Klaus, T. Bland, E. Poli, C. Politi, G. Lamporesi, E. Casotti, R. N. Bisset, M. J. Mark, and F. Ferlaino, Observation of vortices and vortex stripes in a dipolar condensate, Nat. Phys. **18**, 1453 (2022).

[50] T. Bland, G. Lamporesi, M. J. Mark, and F. Ferlaino, Vortices in dipolar Bose-Einstein condensates, arXiv:2303.13263.

[51] P. C. Haljan, I. Coddington, P. Engels, and E. A. Cornell, Driving Bose-Einstein Condensate Vorticity with a Rotating Normal Cloud, Phys. Rev. Lett. **87**, 210403 (2001).

[52] Q. Gu and X. Cui, Self-bound vortex lattice in a rapidly rotating quantum droplet, arXiv:2306.14958.